



Optimal Flight Trajectory to Minimize Noise During Landing

Janav P. Udani,^{*} Kshitij Mall,[†] Michael J. Grant,[‡] and Dengfeng Sun[§]

Purdue University, West Lafayette, IN, 47907

Generally, aircraft performance is judged on the basis of fuel consumption, range, or time criteria, and hence, most optimization studies are carried out on these attributes. With that in mind, any flight event can be segmented into three distinct stages: take-off, cruise and landing. Noise generated by an aircraft during its landing phase is considerably high and, hence, has a significant impact on the population surrounding the airport. While one way to reduce the perceived noise is by reducing the engine noise itself, this study focuses on trajectory optimization to design noise-minimal flight trajectories. In this study, the relationship of the aircraft with its environment during the terminal descent phase has been studied, and optimal control theory and a state of the art trajectory solver, GPOPS-II, have been used to construct noise minimal flight trajectories. The concept of trigonometric is used to implicitly limit the controls and preliminary results solving the 3 degree-of-freedom noise minimization problem are presented. To showcase the impact of population distribution around an airport on the effective perceived noise, an example scenario with a simplistic population distribution function is studied. The higher fidelity problem is solved using optimal control theory and validated through GPOPS-II. The impact of population is reflected by a change in the noise-minimal landing trajectory adopted by the aircraft in this scenario. Additionally, comparisons have been drawn with the flight trajectory simulated using the currently accepted constant descent approach and the cumulative perceived noise is found to be lower for the optimal trajectory. This is the first time optimal control theory has been used to optimize a 3 DOF aircraft landing trajectory problem with three bounded controls.

Nomenclature

ATS	Air Transportation System
BVP	Boundary value problem
CDA	Continuous descent approach
DOF	Degree-of-freedom
EPNL	Effective Perceived Noise Level
EU	European Union
IEPNL	Integral Effective Perceived Noise Level
OCP	Optimal control problem
OCT	Optimal control theory
PDF	Population distribution function
PMP	Pontryagin's Minimum Principle
TPBVP	Two point boundary value problem

^{*}Graduate Student, School of Aeronautics and Astronautics, AIAA Student Member, judani@purdue.edu

[†]Graduate Student, School of Aeronautics and Astronautics, AIAA Student Member mall@purdue.edu

[‡]Assistant Professor, School of Aeronautics and Astronautics, AIAA Senior Member, mjgrant@purdue.edu

[§]Associate Professor, School of Aeronautics and Astronautics, AIAA Senior Member, dsun@purdue.edu

D	Drag force magnitude, N	z	Altitude, m
G	Terminal cost	α	Angle of attack, rad
H	Hamiltonian	α_{TRIG}	Trigonometric angle of attack, rad
J	Cost functional	γ	Flight path angle, rad
L_{COST}	Path cost	$\boldsymbol{\lambda}$	Costate vector
L	Lift force magnitude, N	λ_{γ}	Flight path angle costate, dB/rad
T	Thrust, N	λ_{ψ}	Heading costate, dB/rad
T_{TRIG}	Trigonometric thrust control, rad	λ_v	Velocity costate, dB.s/m
W	Weight, N	λ_x	Downrange costate, dB/m
g	Earth's gravitational acceleration, m/s ²	λ_y	Crossrange costate, dB/m
m	Vehicle mass, kg	λ_z	Altitude costate, dB/m
\mathbf{u}	Control vector	Φ	Terminal constraints
t	Time, s	ϕ	Bank angle, rad
t_f	Final time, s	ϕ_{TRIG}	Trigonometric bank angle, rad
u_{TRIG}	Trigonometric control	Ψ	Initial constraints
v	Velocity magnitude, m/s	ψ	Heading angle
\mathbf{x}	State vector		
x	Downrange, m		
y	Crossrange, m		

I. Introduction

OPTIMIZATION of flight trajectories is an area of vital importance in air traffic management from the operations point of view. Generally, studies under this topic aim to define optimal flight paths that ultimately lead to energy-efficient flights.¹ Noise of commercial aircraft has been a cause of serious concern for the population around airports.² This problem is manifested during night-time operations when an aircraft significantly disturbs the surrounding area. While constant descent approach (CDA) is a possible solution,³ many countries impose night flying restrictions wherein the airport is closed and no aircraft operations can take place. Hence, if an aircraft is scheduled to land at a particular airport, the flight either has to be cancelled at the airport of origin, or the aircraft has to be diverted to the nearest airport that is open for night-time operations. Such laws become a serious impediment, especially in the European Union (EU) where almost all airports do not permit night-time operations.⁴ The cost incurred due to these impediments is likely to be high.

Improvement of engine characteristics as well as development of new flight paths are two solutions that reduce aircraft noise.^{1,5} The goal of this investigation is to maintain the high safety standards of flight operations when designing new flight paths that minimize noise.² To this end, an optimal control problem (OCP) is formulated and solved to minimize the noise of an aircraft during landing. A system of ordinary differential equations is used to represent the flight dynamics of an aircraft along with some safety and comfort constraints that are used in general practice to satisfy public transport requirements.^{6,7} A real world noise minimal aircraft landing problem is simulated and solved by imposing realistic bounds on the controls using the concept of trigonometrization, which has not been done before.⁸ Previously, a 2 degree-of-freedom (DOF) study was carried out on noise minimization aircraft trajectories whereas this study focuses on a more complicated and realistic 3 DOF case. Subsequently, a cost functional is defined which aims to minimize the noise index of an aircraft landing event.^{2,5,9}

Section II outlines the concepts used in this study. An example 3 DOF landing problem is solved to minimize noise in Section III and a simplistic population distribution function (PDF) is discussed in Section IV. Additionally, in Section IV, initial comparisons are drawn between the proposed trajectory and the trajectory generated by simulating CDA.

II. Preliminaries

II.A. Necessary Conditions of Optimality using Calculus of Variations

OCPs involve the calculation of the time-history of the control variable(s) associated with a system that optimizes a given performance index while satisfying problem-specific constraints at the initial point, terminal point, and interior points as well as path constraints. An OCP is generally expressed in the form given in Eq. (1). J is the cost functional, with G being the terminal cost and $\int_{t_0}^{t_f} L_{\text{COST}}(\mathbf{x}, \mathbf{u}, t) dt$ being the path cost. There are also initial and terminal constraints, Ψ and Φ respectively, that are to be satisfied simultaneously.

$$\text{Min } J = G(\mathbf{x}(t_f), t_f) + \int_{t_0}^{t_f} L_{\text{COST}}(\mathbf{x}, \mathbf{u}, t) dt \quad (1)$$

Subject to:

$$t_0 = 0$$

$$\dot{\mathbf{x}} = \mathbf{f}(\mathbf{x}, \mathbf{u}, t) \quad (2)$$

$$\Psi(\mathbf{x}(t_0), t_0) = 0 \quad (3)$$

$$\Phi(\mathbf{x}(t_f), t_f) = 0 \quad (4)$$

Indirect methods optimize the cost functional J shown in Eq. (1) by formulating a Two-Point Boundary Value Problem (TPBVP) that represents the necessary conditions of optimality. If these boundary conditions are satisfied, the solution will be locally optimal in the design space. In order to do this, the dynamic equations of the system are augmented with a set of costates, and the necessary conditions of optimality are formulated by applying the Euler-Lagrange equation.¹⁰

The Hamiltonian is defined as shown in Eq. (5), where λ is the costate vector with its corresponding dynamic equations defined in Eq. (6). The optimal control law, $\mathbf{u}(t)$, is obtained as a function of the states and costates by solving Eq. (7). The initial and terminal boundary conditions on the costates are specified in Eqs. (8) and (9), where ν_0 and ν_f are sets of undetermined parameters which are used to adjoin these boundary conditions to the cost functional. The time of flight of the trajectory is determined by the free final time condition shown by Eq. (10). The necessary conditions of optimality are defined by Eqs. (6–10), and they form a well-defined TPBVP that can be solved using BVP solvers.

$$H = L(\mathbf{x}, \mathbf{u}, t) + \lambda^T(t) \mathbf{f}(\mathbf{x}, \mathbf{u}, t) \quad (5)$$

$$\dot{\lambda} = -\frac{\partial H}{\partial \mathbf{x}} \quad (6)$$

$$\frac{\partial H}{\partial \mathbf{u}} = 0 \quad (7)$$

$$\lambda(t_0) = \nu_0^T \frac{\partial \Psi}{\partial \mathbf{x}(t_0)} \quad (8)$$

$$\lambda(t_f) = \left(\frac{\partial G}{\partial \mathbf{x}(t_f)} + \nu_f^T \frac{\partial \Phi}{\partial \mathbf{x}(t_f)} \right) \quad (9)$$

$$\left(H + \frac{\partial G}{\partial t} + \nu_f^T \frac{\partial \Phi}{\partial t} \right)_{t=t_f} = 0 \quad (10)$$

II.B. Pontryagin's Minimum Principle

When more than one option exists after solving Eq. (7), the optimal control is chosen using Pontryagin's Minimum Principle (PMP) as shown in Eq. (11), where * refers to the optimal value.¹⁰ It states that the optimal control will minimize the Hamiltonian, H , for all admissible values of control.¹⁰

$$H(t, \mathbf{x}^*(t), \mathbf{u}^*(t), \lambda^*(t)) \leq H(t, \mathbf{x}^*(t), \mathbf{u}(t), \lambda^*(t)) \quad (11)$$

II.C. Trigonomerization of Bounded Control Problems

The concept of trigonomerization⁸ is used to express the control in the form of trigonometric functions, which are bounding in nature. This concept is applicable for any bounded control problem.¹¹ Trigonomerization can be applied to OCPs where the Hamiltonian is given by Eq. (12), where $f(u)$ is a non-linear function of u .

$$H = H_0(t, x, \lambda) + H_1(t, x, \lambda)f(u) \quad (12)$$

Suppose the control for an OCP is represented originally as u . If u is bounded, it can be rewritten in a bounded form using trigonomerization as shown in Eqs. (13), where $u_{\text{LowerBound}}$ and $u_{\text{UpperBound}}$ are the lower and upper bounds on u , respectively. This trigonometric reformulation greatly simplifies problem formulation and solution process for OCPs.

$$u_1 = \frac{u_{\text{UpperBound}} - u_{\text{LowerBound}}}{2} \quad (13a)$$

$$u_0 = \frac{u_{\text{UpperBound}} + u_{\text{LowerBound}}}{2} \quad (13b)$$

$$u = u_1 \sin u_{\text{TRIG}} + u_0 \quad (13c)$$

Trigonomerization also avoids solving a multi-point boundary value problem by allowing the problem to remain a TPBVP. This significantly reduces the effort required for problem formulation and solution process. Moreover, this investigation warrants the use of three controls that require realistic bounding for obtaining noise minimal flight trajectories.

III. Noise-Minimal 3 DOF Trajectory Optimization

To design minimal noise trajectories, a suitable noise index must be selected. The general aircraft noise indices, which effectively describe the noise during an aircraft landing event, are Sound Exposure Level, Overall Sound Pressure Level,¹² Effective Perceived Noise Level (EPNL), and Equivalent Noise Level.² Minimization of the EPNL (i.e., the noise perceived by a person standing at a fixed distance from the aircraft) is chosen for this problem. In any aircraft landing event,⁵ it is necessary to consider the person who is nearest to the aircraft as it is that person who is affected most by the aircraft's noise. Hence, the noise index is a function of the altitude, z . This function represents the zoning-plan of the community surrounding the airport and can be approximated as $(z+50)$.⁵

It is also necessary to consider the duration for which the noise lasts. Hence, minimization of the EPNL⁵ is chosen. Thus, the cost functional is to minimize the EPNL over the entire trajectory. It is termed as Integral Effective Perceived Noise Level (IEPNL) and is shown in Eq. (14a).⁵ The equations of motion describing a 3 DOF trajectory of an aircraft are used for this problem as shown in Eqs. (14b)-(14g).⁶ The lift force, L , and the drag force, D , are approximated as shown in Eq. (14h) and Eq. (14i), respectively.^{1,5}

Minimize:

$$J = \int_0^{t_f} \frac{18.73 T^{5.2}}{v(z+50)^{2.5}} \cos \gamma dt \quad (14a)$$

Subject to:

$$\dot{x} = v \cos \gamma \cos \psi \quad (14b)$$

$$\dot{y} = v \cos \gamma \sin \psi \quad (14c)$$

$$\dot{z} = v \sin \gamma \quad (14d)$$

$$\dot{v} = \frac{T \cos \alpha - D}{m} - g \sin \gamma \quad (14e)$$

$$\dot{\psi} = \frac{(T \sin \alpha + L) \sin \phi}{mv \cos \gamma} \quad (14f)$$

$$\dot{\gamma} = \frac{(T \sin \alpha + L) \cos \phi}{mv} - \frac{g \cos \gamma}{v} \quad (14g)$$

$$L = W = mg \quad (14h)$$

$$D = c_1 v^2 + \frac{c_2}{v^2} \quad (14i)$$

In the above equation, J is the noise minimization cost functional, x is the downrange, y is the crossrange, z is the altitude, v is the velocity, ψ is the heading angle, γ is the flight path angle, m is the mass of the vehicle, D is the drag force magnitude, L is the lift force magnitude, ϕ is the bank angle, α is the angle of attack, and T is the thrust force magnitude. The constants used in this problem, as shown in Table 1, are the weight of the aircraft, W , the acceleration due to Earth's gravity, g , and constants related to the drag force, c_1 and c_2 . This problem is particularly difficult to solve because the general tendency to minimize noise based on the cost function (as shown in Eq. (14a)) would be to fly at high altitudes with low thrust and high velocity. While considering a landing event, not only the altitude but also the velocity must decrease to satisfy operational constraints, which would inevitably lead to an increase in the noise level.⁹

Table 1: Parameters for aircraft's noise-minimal trajectory problem.

Parameter (Unit)	Value
c_1 (kg/m)	0.226
c_2 (kg m ³ /s ⁴)	5.2e6
W (N)	7180
g (m/s ²)	9.81

Using trigonumerization, the bank angle and the angle of attack are written as shown in Eqs. (15a) and (15b), respectively. The bounds on the bank angle and angle of attack are chosen as $\pm 60^\circ$ ($\pm \pi/3$) and $\pm 15^\circ$ ($\pm \pi/12$), respectively. Thrust can similarly be trigonumerized as shown in (15c) with a lower bound of 300 N and an upper bound of 3420 N.⁵

$$\phi = \frac{\pi}{3} \sin \phi_{\text{TRIG}} \quad (15a)$$

$$\alpha = \frac{\pi}{12} \sin \alpha_{\text{TRIG}} \quad (15b)$$

$$T = 1560 \sin T_{\text{TRIG}} + 1860 \quad (15c)$$

The Hamiltonian for this problem can be written as shown in Eq. (16). The equations of motion corresponding to the costates can then be evaluated using Eqs. (6) and are shown in Eq. (17).

$$H = \frac{18.73 T^{5.2}}{v(z+50)^{2.5}} \cos \gamma + \lambda_x (v \cos \gamma \cos \psi) + \lambda_y (v \cos \gamma \sin \psi) + \lambda_z (v \sin \gamma) + \lambda_v \left(\frac{T \cos \alpha - D}{m} - g \sin \gamma \right) + \lambda_\psi \left(\frac{(T \sin \alpha + L) \sin \phi}{mv \cos \gamma} \right) + \lambda_\gamma \left(\frac{(T \sin \alpha + L) \cos \phi}{mv} - \frac{g \cos \gamma}{v} \right) \quad (16)$$

$$\dot{\lambda}_x = 0 \quad (17a)$$

$$\dot{\lambda}_y = 0 \quad (17b)$$

$$\dot{\lambda}_z = \frac{46.825 T^{5.2}}{v(z+50)^{3.5}} \cos \gamma \quad (17c)$$

$$\begin{aligned} \dot{\lambda}_v = & \frac{18.73 T^{5.2}}{v^2(z+50)^{2.5}} \cos \gamma - \lambda_x(\cos \gamma \cos \psi) - \lambda_y(\cos \gamma \sin \psi) - \lambda_z(\sin \gamma) \\ & + 2\lambda_v \left(\frac{c_1 v^4 - c_2}{m v^3} \right) + \lambda_\psi \left(\frac{(T \sin \alpha + L) \sin \phi}{m v^2 \cos \gamma} \right) + \lambda_\gamma \left(\frac{(T \sin \alpha + L) \cos \phi}{m v^2} - \frac{g \cos \gamma}{v^2} \right) \end{aligned} \quad (17d)$$

$$\dot{\lambda}_\psi = \lambda_x(v \cos \gamma \sin \psi) - \lambda_y(v \cos \gamma \cos \psi) \quad (17e)$$

$$\begin{aligned} \dot{\lambda}_\gamma = & \frac{18.73 T^{5.2}}{v(z+50)^{2.5}} \sin \gamma + \lambda_x(v \sin \gamma \cos \psi) + \lambda_y(v \sin \gamma \sin \psi) - \lambda_z(v \cos \gamma) \\ & + \lambda_v g \cos \gamma - \lambda_\psi \left(\frac{(T \sin \alpha + L) \sin \phi \sin \gamma}{m v \cos^2 \gamma} \right) - \lambda_\gamma \frac{g \sin \gamma}{v} \end{aligned} \quad (17f)$$

Using OCT, the optimal control options obtained for this problem are shown in Eqs. (18), (19), and (20) for bank angle, angle of attack, and thrust control, respectively. PMP as described in Eq. (11) can then be used to choose the optimal combination of controls from among these options. Preliminary results obtained for an example case are presented in the next section.

$$\phi_{TRIG}^* = \begin{cases} -\frac{\pi}{2} \\ \arcsin \left(\frac{\arctan \left(\frac{\lambda_\psi}{\lambda_\gamma \cos \gamma} \right)}{\frac{\pi}{3}} \right) \\ \arcsin \left(\frac{\arctan \left(\frac{\lambda_\psi}{\lambda_\gamma \cos \gamma} \right) + \pi}{\frac{\pi}{3}} \right) \\ \frac{\pi}{2} \end{cases} \quad (18)$$

$$\alpha_{TRIG}^* = \begin{cases} -\frac{\pi}{2} \\ \arcsin \left(\frac{\arctan \left(\frac{\lambda_\psi \sin \phi}{v \lambda_v \cos \gamma} + \frac{\lambda_\gamma \cos \phi}{v \lambda_v} \right)}{\frac{\pi}{12}} \right) \\ \arcsin \left(\frac{\arctan \left(\frac{\lambda_\psi \sin \phi}{v \lambda_v \cos \gamma} + \frac{\lambda_\gamma \cos \phi}{v \lambda_v} \right) + \pi}{\frac{\pi}{12}} \right) \\ \frac{\pi}{2} \end{cases} \quad (19)$$

$$T_{TRIG}^* = \begin{cases} -\frac{\pi}{2} \\ \arcsin \left(\frac{\left(\frac{v(z+50)^{2.5}}{97.396 \cos \gamma} \left(-\frac{\lambda_v \cos \alpha}{m} - \frac{\lambda_\psi \sin \alpha \sin \phi}{m v \cos \gamma} - \frac{\lambda_\gamma \sin \alpha \cos \phi}{m v} \right) \right)^{\frac{1}{4.2}} - 1860}{1560} \right) \\ \frac{\pi}{2} \end{cases} \quad (20)$$

It can be seen in Eqs. (19) that the optimal values of bank angle, ϕ^*_{TRIG} , are required to evaluate the optimal values of the angle of attack, α^*_{TRIG} . Similarly, ϕ^*_{TRIG} and α^*_{TRIG} are necessary to evaluate optimal thrust control, T^*_{TRIG} , as shown in Eqs. (20). Thus, it is mandatory to evaluate the optimal bank angle first, followed by the optimal angle of attack and lastly the optimal value of thrust. It can also be seen that there are four options for optimal bank angle, four options for optimal angle of attack and three options for optimal thrust, resulting in a total of 48 optimal control options to select from using PMP.

III.A. Preliminary Results

An example scenario is presented and solved for the initial and final conditions enforced upon the aircraft trajectory as shown in Table 2. The values in this table are derived from a 2 DOF problem described in Ref. 5 as a benchmark.

Table 2: Initial and final conditions for aircraft's noise-minimal trajectory problem.

Attribute	Initial Value	Final Value
Time (s)	0	free
Downrange (km)	0	5.4
Crossrange (km)	0	4.6
Altitude (km)	1.197	0
Velocity (m/s)	124	77.5
Heading Angle ($^\circ$)	0	45
Flight Path Angle ($^\circ$)	0	0

The results have been obtained using OCT by satisfying necessary conditions of optimality and also by using a state of the art trajectory optimizer based on pseudospectral method, GPOPS-II.¹³ The 3D trajectory plot and the noise generated by the aircraft are shown in Fig. 1. The IEPNL generated by the aircraft is found to be 6395 dB-s.^{1,5} The time histories of the states are shown in Fig. 2. The velocity along the trajectory is within the acceptable range for comfort and safety of the passengers.

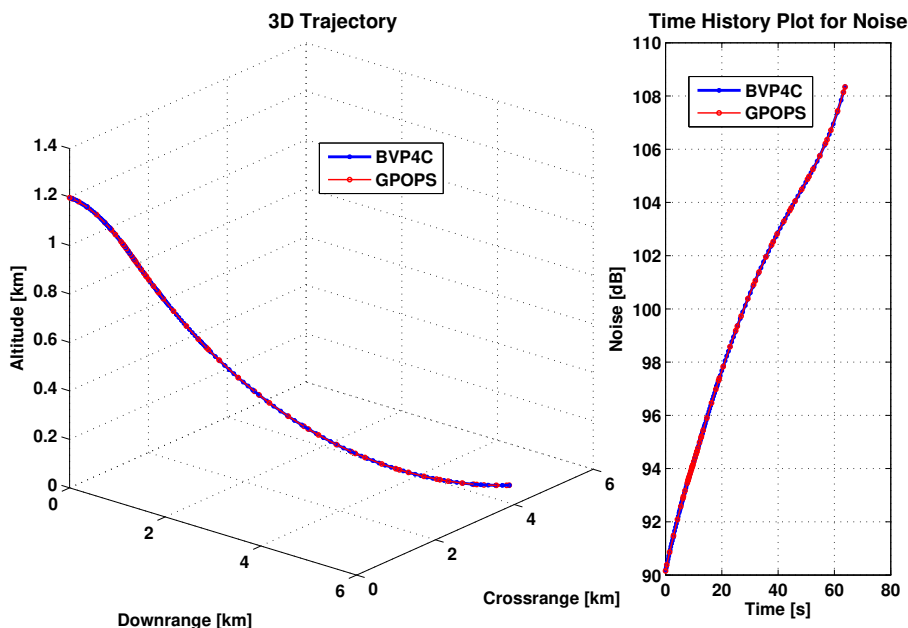


Figure 1: 3D trajectory and noise history for the aircraft.

The control history plots for the bank angle, the angle of attack, and the thrust are shown in Fig. 3. It can be seen that these controls stay within the required bounds. Fig. 4 shows that the magnitudes of the costates are extremely high, thus highlighting the need to scale the problem under consideration. However, no scaling has been employed to solve this problem in its current form, which goes to show the robustness of

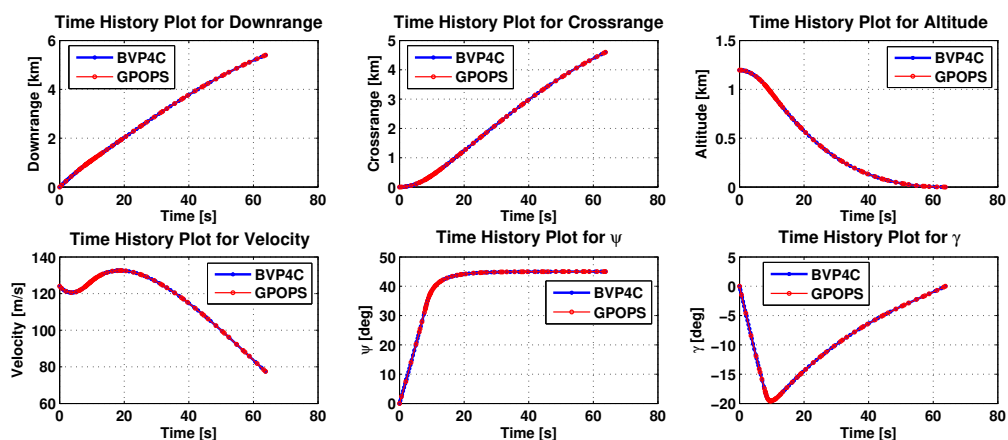


Figure 2: Time histories of states.

the solver employed. It should also be noted that a different combination of costates from GPOPS-II results in the same optimal controls, and, hence, there is a difference in the costates between OCT and GPOPS-II as shown in Fig. 4.

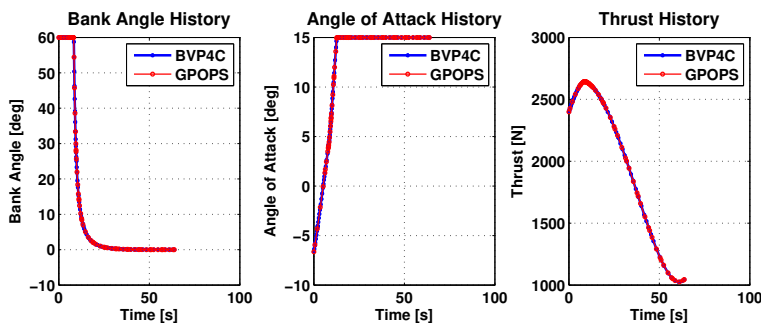


Figure 3: Time histories of controls.

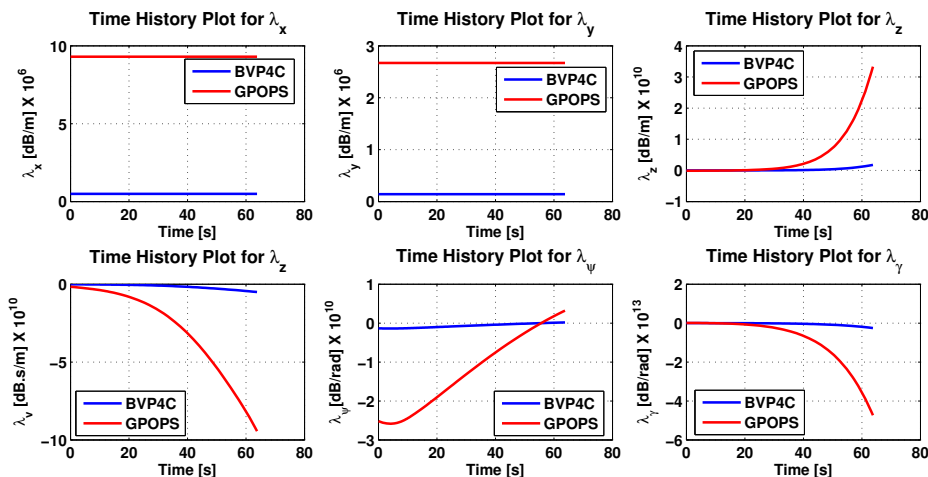


Figure 4: Time histories of costates.

This is the first time that an aerospace problem with six states and three bounded controls, as presented in this study, has been solved using trigonumerization. This sets the confidence to increase the fidelity of the noise minimization functional by incorporating a population model, thus accounting for a more realistic

perceived noise, as described in the next section.

IV. Higher Fidelity Population Model

In the prior example, the cost functional minimized is the IEPNL as perceived by the person nearest to the aircraft. In order to model and simulate a realistic scenario, it is important to incorporate the population distribution around the airport. If the latitudinal and the longitudinal coordinate data corresponding to the area around the airport is available, a polynomial function can be used to model the population data. This equation, when multiplied with the noise model, yields a weighted cost functional that is representative of the noise perceived by the total number of people in an area rather than the noise perceived when considering unit population distribution. Such a weighted cost functional will ensure that minimum number of people are affected by the aircraft's noise during its terminal descent. The modified cost functional is given by Eq. (21), which is essentially the product of Eq. (14a) and the PDF.

$$J = \int_0^{t_f} (\text{PDF}) \frac{18.73 T^{5.2}}{v(z+50)^{2.5}} \cos \gamma dt \quad (21)$$

Due to unavailability of the aforementioned coordinate data for the population model, we have employed a general polynomial function as shown in Eq. (22) which is representative of a population change as the aircraft flies towards the airport. This non-linear function models the population variation based on the changes in the crossrange.

$$\text{PDF} = \frac{4600}{y+1} \quad (22)$$

The problem formulation is similar to Sec. III except the objective functional is given by Eq. (21), where the PDF is as shown in Eq. (22). The optimal control law is modified only for thrust and is shown in Eq. (23). Also, the modified equations of motion for the costates for this scenario are shown in Eqs. (24a)-Eqs. (24d). It should be noted that the costates for downrange, x , and heading angle, ψ , remain unmodified.

$$T_{TRIG}^* = \begin{cases} -\frac{\pi}{2} \\ \arcsin \left(\frac{\left(\frac{v(1+y)(z+50)^{2.5}}{448021.6 \cos \gamma} \left(-\frac{\lambda_v \cos \alpha}{m} - \frac{\lambda_\psi \sin \alpha \sin \phi}{mv \cos \gamma} - \frac{\lambda_\gamma \sin \alpha \cos \phi}{mv} \right) \right)^{\frac{1}{4.2}} - 1860}{1560} \right) \\ \frac{\pi}{2} \end{cases} \quad (23)$$

$$\dot{\lambda}_y = \frac{86158 T^{5.2}}{v(1+y)^2(z+50)^{2.5}} \cos \gamma \quad (24a)$$

$$\dot{\lambda}_z = \frac{215395 T^{5.2}}{v(1+y)(z+50)^{3.5}} \cos \gamma \quad (24b)$$

$$\begin{aligned} \dot{\lambda}_v = & \frac{86158 T^{5.2}}{v^2(1+y)(z+50)^{2.5}} \cos \gamma - \lambda_x(\cos \gamma \cos \psi) - \lambda_y(\cos \gamma \sin \psi) - \lambda_z(\sin \gamma) \\ & + 2\lambda_v \left(\frac{c_1 v^4 - c_2}{mv^3} \right) + \lambda_\psi \left(\frac{(T \sin \alpha + L) \sin \phi}{mv^2 \cos \gamma} \right) + \lambda_\gamma \left(\frac{(T \sin \alpha + L) \cos \phi}{mv^2} - \frac{g \cos \gamma}{v^2} \right) \end{aligned} \quad (24c)$$

$$\begin{aligned} \dot{\lambda}_\gamma = & \frac{86158 T^{5.2}}{v(1+y)(z+50)^{2.5}} \sin \gamma + \lambda_x(v \sin \gamma \cos \psi) + \lambda_y(v \sin \gamma \sin \psi) - \lambda_z(v \cos \gamma) \\ & + \lambda_v g \cos \gamma - \lambda_\psi \left(\frac{(T \sin \alpha + L) \sin \phi \sin \gamma}{mv \cos^2 \gamma} \right) - \lambda_\gamma \frac{g \sin \gamma}{v} \end{aligned} \quad (24d)$$

A comparison is drawn between the results obtained while considering the effect of the PDF given by Eq. (22) and the results obtained in Sec. III. The 3D trajectory and noise history plots as shown in Fig. 5 indicate a different flight path adopted by the aircraft resulting in a higher noise. The IEPNL obtained is 6860 dB-s. This is expected as the PDF in this scenario has significantly higher magnitudes than the uniform population distribution investigated previously.

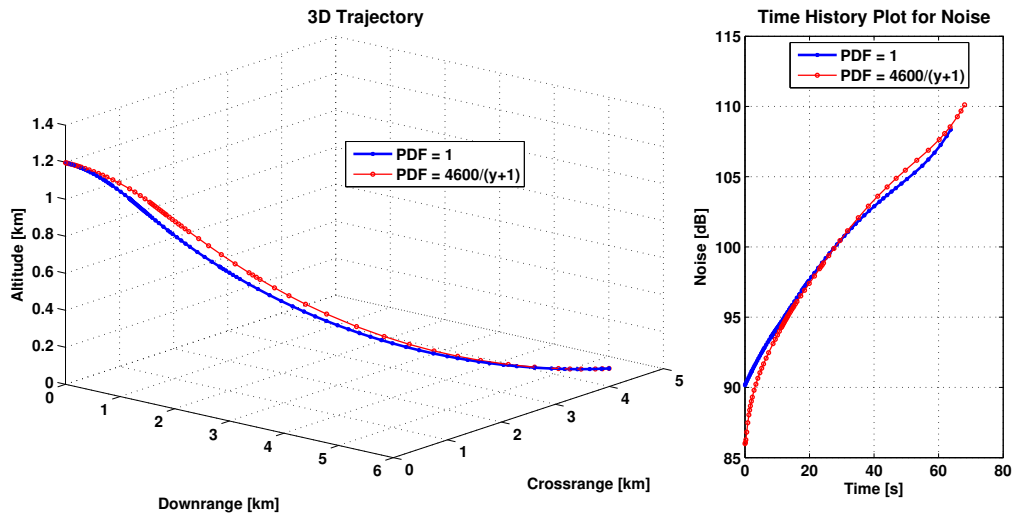


Figure 5: Comparison of 3D trajectory and noise history for the aircraft.

Since the population is very high initially in the crossrange direction, the aircraft flies a higher altitude trajectory to minimize the total perceived noise. This can be easily seen in the state history plots as shown in Fig. 6. Given the final state constraints, the aircraft is forced to utilize extremal controls to follow the optimal trajectory as seen in Fig. 7. OCT requires the costates to be of high magnitudes in order to obtain such extremal controls. The costates history plots as shown in Fig. 8 are consistent with the expected results.

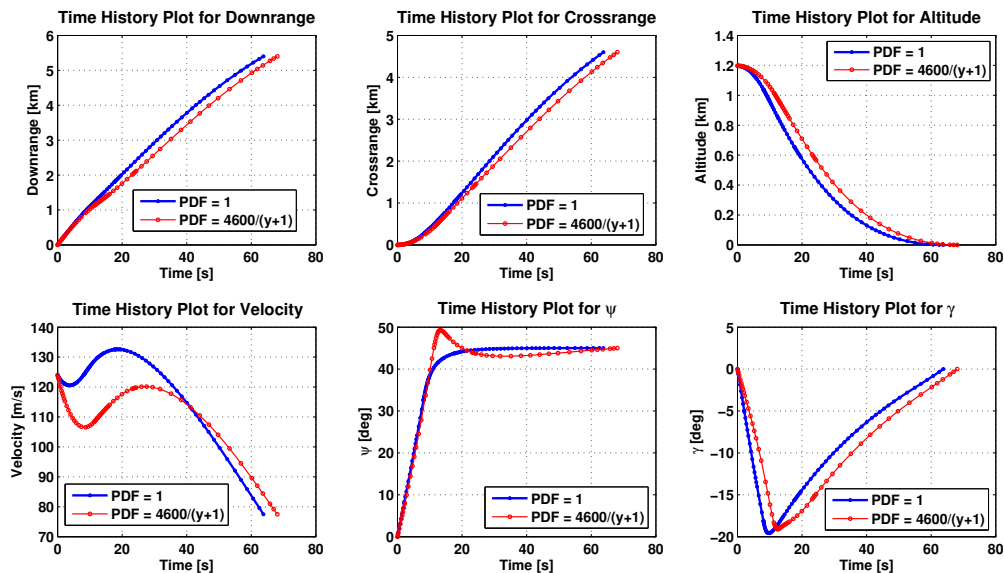


Figure 6: Comparison of time histories of states.

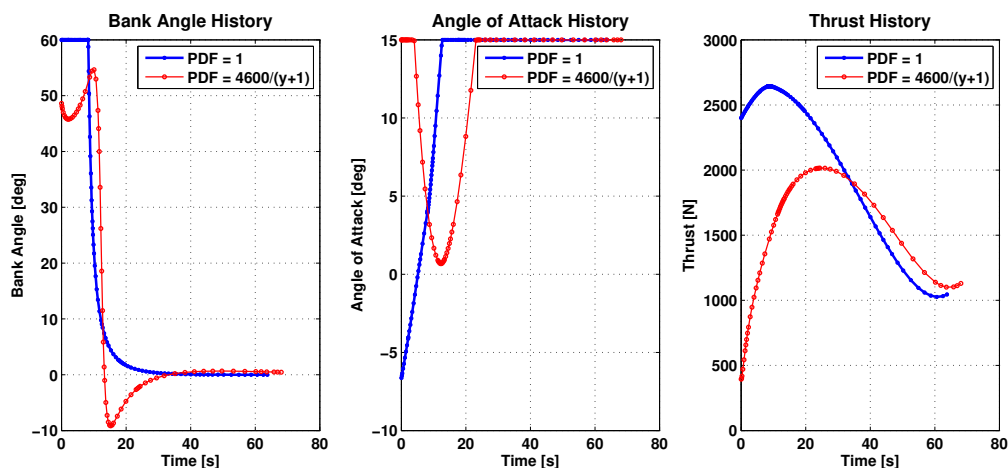


Figure 7: Comparison of time histories of controls.

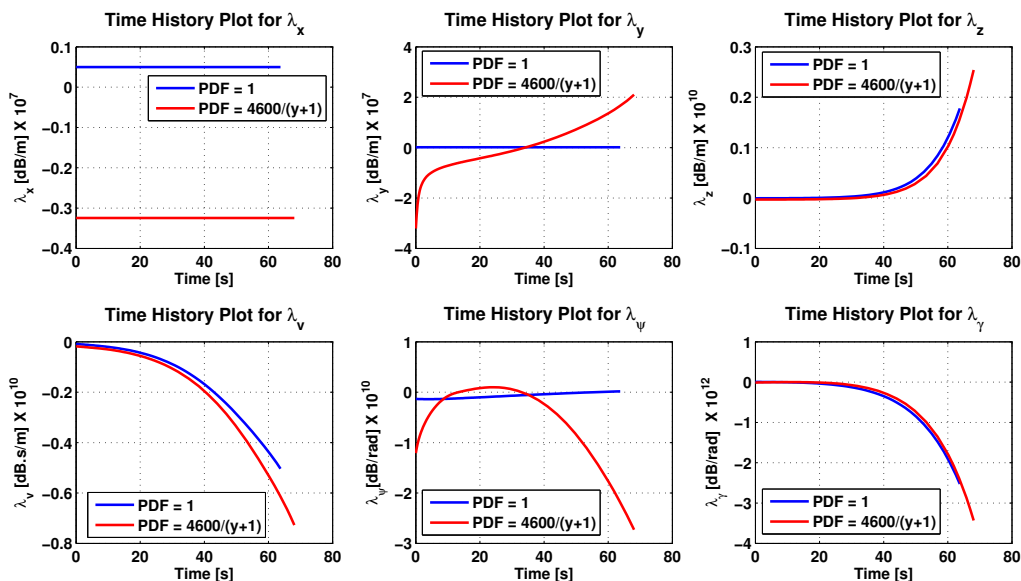


Figure 8: Comparison of time histories of costates.

Additionally, to study the practicability of the proposed method it is interesting to draw comparisons with the currently accepted CDA. The flight trajectory employing CDA has been simulated using equations of motion as described in Eqs.(14b)-Eqs. (14f) and the constant parameters as described in Table 3. The optimal noise trajectory reduces the IEPNL by approximately 7% over CDA. The simulated CDA trajectory and corresponding noise history are compared with the optimal results in Fig. 9.

Table 3: Constant parameters for CDA.

Parameter	Value
Angle of attack ($^\circ$)	10
Bank angle ($^\circ$)	12.5
Thrust (N)	1700
Flight path angle ($^\circ$)	-8.5

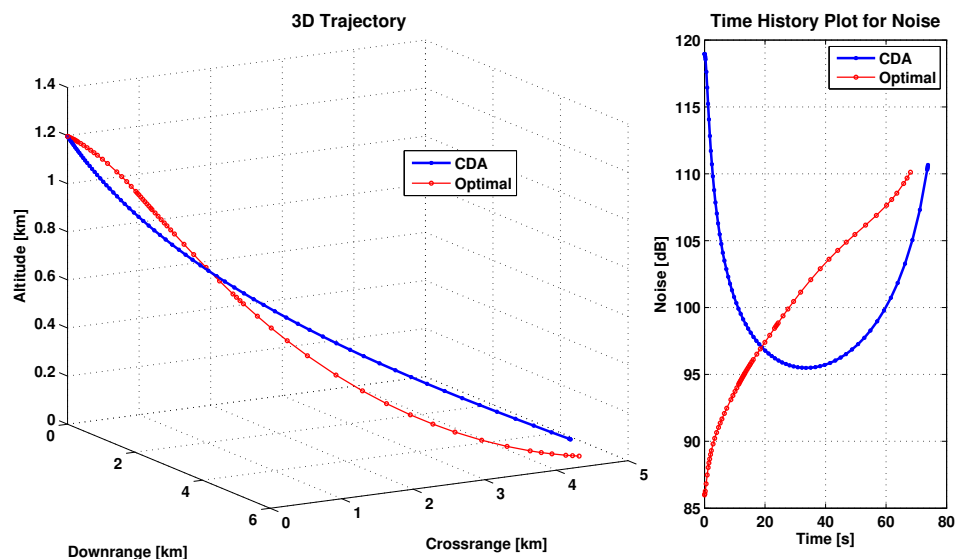


Figure 9: Comparison of 3D trajectory and noise history of the aircraft between optimal approach and CDA.

V. Conclusion

A 3 DOF flight trajectory problem to find minimal noise trajectories for an aircraft during its terminal descent phase is presented and solved. OCT along with trigonometric optimization is used to find the solution as OCT is based on satisfying necessary conditions of optimality, thus guaranteeing a high-quality solution. State of the art software, GPOPS-II, which is based on the pseudo-spectral method, has also been used to find the solution, and an excellent agreement is observed between the results found by the two solvers. To demonstrate the effect of variable population on the noise optimal trajectories of the aircraft, an example scenario has been presented with a simplistic PDF. The considered scenario is solved using OCT and yields a relatively different 3D trajectory to the original problem that does not take population into account while calculating total perceived noise. Comparisons drawn with the CDA trajectory reveal that the IEPNL is indeed minimized. Thus, this study lays the foundation for assessing the practicability of constrained night time operations, especially cargo operations. This study gains high relevance in the current scenario where the NextGen air transportation system (ATS) is being developed, part of which aims to reduce noise pollution.

VI. Future Work

The ultimate goal of this study involves proposing and assessing the practicability of new noise-minimal flight paths for an aircraft during the terminal descent phase around real world airports. One such airport is Hartsfield-Jackson international airport in Atlanta and the population distribution around this airport is shown in Fig. 10.

The population data is retrieved from Ref.14 and is based on the 2010 census.¹⁵ Interesting flight trajectories circumnavigating high population zones are expected around such an airport to minimize the total perceived noise. The current research is undertaken to explore optimal solutions without very strict restrictions on the state variables. The future work also involves incorporating enhanced constraints on the state variables imposed by taking passenger comfort into account as required by NextGen ATS.

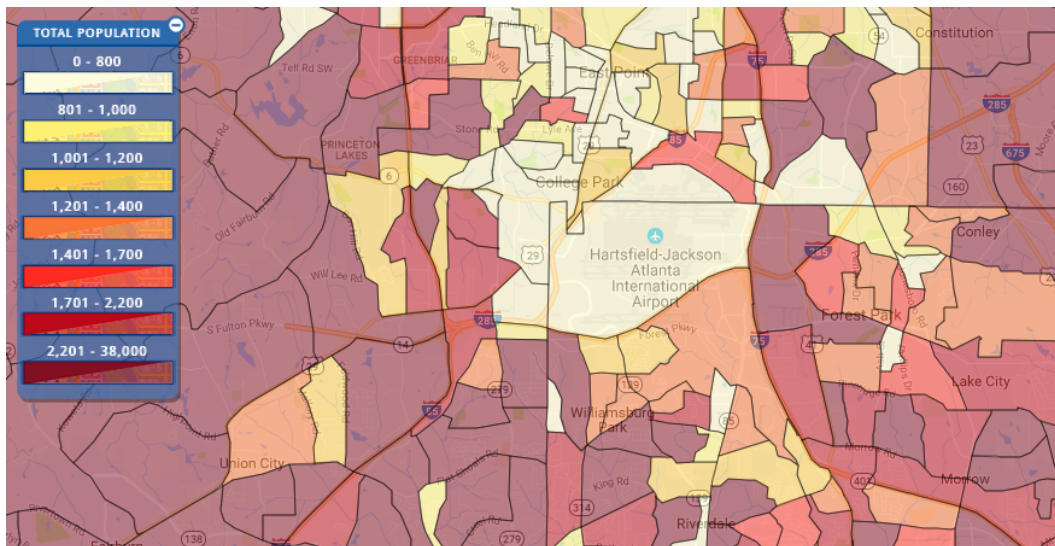


Figure 10: Population distribution model for Hartsfield-Jackson airport, Atlanta.

References

- ¹Ohta, H. "Analysis of Minimum Noise Landing Approach Trajectory," *Journal of Guidance, Control, and Dynamics*, Vol. 5, No. 3, 1982, pp. 263-269.
- ²Abdallah, L., "Optimal Flight Paths Reducing the Aircraft Noise during Landing," *MCO* Oct. 25, 2008, pp. 1-10.
- ³Gatwick, B.L., "Flight Evaluation Report 2007," *British Airports Authority*, 2007.
- ⁴"Night Flight Restrictions," *Worldwide Air Transport Conference (ATCONF)*, URL: <http://www.icao.int/Meetings/atconf6/Documents/WorkingPapers/> [cited 13 Dec. 2016].
- ⁵Kugelmann, B., "Minimizing the Noise of an Aircraft During Landing Approach," *Variational Calculus, Optimal Control and Applications*, pp. 271-280.
- ⁶Vinh N., *Optimal Trajectories in Atmospheric Flight*, Elsevier, Vol. 2, 2 Dec. 2012.
- ⁷Abdallah, L., Haddou, M., and Khaldi, S., "Optimization of Operational Aircraft Parameters Reducing Noise Emission," *Applied Mathematical Sciences*, Vol. 4, No. 11, 2010, pp. 515-535.
- ⁸Mall, K. and Grant, M. J., "Trigonometrization of Optimal Control Problems with Bounding Controls," *AIAA Aviation Forum and Exposition*, Washington, D. C., 13-17 Jun. 2016.
- ⁹Reynolds, T.G., Ren, L., Clarke, J.P.B., Burke, A.S. and Green, M., "History, Development and Analysis of Noise Abatement Arrival Procedures for UK Airports," *AIAA Fifth Aviation, Technology, Integration and Operations Conference*, Arlington, VA, Sept. 2005.
- ¹⁰Longuski, J. M., Guzman, J. J., and Prussing, J. E., *Optimal Control with Aerospace Applications*, 1st ed., Springer, New York, 2014.
- ¹¹Mall, K. and Grant, M. J., "Epsilon-Trig Regularization Method for Bang-Bang Optimal Control Problems," *AIAA Aviation Forum and Exposition*, Washington, D. C., 13-17 Jun. 2016.
- ¹²Alam, S., Nguyen, M. H., Abbass, H. A., Lokan, C., Ellejmi, M., and Kirby, S., "A Dynamic Continuous Descent Approach Methodology for Low Noise and Emission," *Digital Avionics Systems Conference (DASC)*, 2010 IEEE/AIAA 29th. IEEE, Oct. 2010.
- ¹³Patterson, M. A. and Rao, A. V., "GPOPS-II: A MATLAB Software for Solving Multiple-Phase Optimal Control Problems Using hp-Adaptive Gaussian Quadrature Collocation Methods and Sparse Nonlinear Programming," *ACM Transactions on Mathematical Software*, Vol. 41, No. 1, Article No. 1, Oct. 2014, pp. 1:1 - 1:37.
- ¹⁴"2010 Census Interactive Population Map," *US Census Bureau* [online database], URL: <http://www.census.gov/2010census/popmap/> [cited 13 Dec. 2016].
- ¹⁵Clarke, J. P. B., "Systems Analysis of Noise Abatement Procedures Enabled by Advanced Flight Guidance Technology," *Journal of Aircraft*, Vol. 37, No. 2, 2000, pp. 266-273.